The interaction of oxygen with the surface of CeO2-TiO2 mixed systems: An example of fully reversible surface-to-molecule electron transfer

PCCP

Accepted Manuscript

ROYAL SOCIETY OF CHEMISTRY

www.rsc.org/pccp

Cite this: DOI: 10.1039/c0xx00000x

www.rsc.org/xxxxxx

ARTICLE TYPE

The interaction of oxygen with the surface of CeO_2-TiO_2 mixed systems: an example of fully reversible surface-to-molecule electron transfer.

Chiara Gionco,[a] Elio Giamello,[a] Lorenzo Mino[a] and Maria Cristina Paganini*[a]

Received (in XXX, XXX) Xth XXXXXXXXX 20XX, Accepted Xth XXXXXXXXX 20XX

DOI: 10.1039/b000000x

The interaction of oxygen with the surface of CeO_2-TiO_2 mixed oxides prepared via sol-gel was investigated by means of electron paramagnetic resonance (EPR). Upon admission of molecular oxygen onto the surface of the as prepared materials (which underwent a final oxidative calcinations) the formation of superoxide O_2^- ions is observed with no need of preliminary annealing in vacuum and consequent oxygen depletion. The superoxide species is symmetrically adsorbed ("side-on" structure) on the top of a Ce^{4+} ion. Surprisingly the electron transfer is fully reversible at room temperature having the typical behavior shown by molecular oxygen carriers, which, however, link to oxygen in a completely different manner ("end-on" structure). We suggest that the active sites are Ce^{3+} ions present in the stoichiometric cerium titanate which forms during the synthesis. The features of these Ce^{3+} ions must be different from those of the same ions formed in CeO_2 by reductive treatments and which show a different reactivity with O_2. The observation here reported opens innovative perspectives in the field of heterogeneous catalysis and in that of sensors as the total reversibility of the electron transfer is observed in a significant range of oxygen pressure.

Introduction

The adsorption of oxygen onto the surface of metal oxides is a subject of considerable importance in various fields of chemistry and materials science. In particular, selective oxidation catalysis is based on the delicate interplay between the capacity of a reducible oxide to insert oxygen in organic substrates and that of reincorporate the lost lattice oxygen reducing the molecules of O_2 present in the reaction mixture. This is known under the name of Mars-Van Krevelen mechanism[1].

Among reducible oxides CeO_2 has been widely studied because of its unique ability to easily release and reincorporate oxygen that makes this oxide an excellent active support in three way catalysts (TWC) for automobile exhaust remediation[2] and as oxygen sensor[3]. The ceria activity of oxygen storage and release is accompanied by the fluctuation of Ce ions from reduced (Ce^{3+}) to oxidized (Ce^{4+}) states. Both the need of modulating the oxygen storage properties in TWC and that of optimizing the thermal stability of the catalytic systems has recently prompted an intense investigation of mixed systems in which ceria is coupled with other less reducible (or non reducible) oxides such as ZrO_2[4-12], Al_2O_3[13, 14], TiO_2[8, 15-17].

Basic studies on the surface chemistry of metal oxides have shown that the incorporation of oxygen into an oxide matrix occurs with the progressive reduction of O_2, whose first stage is the formation of adsorbed superoxide O_2^- ions. This paramagnetic intermediate (hardly detectable by other techniques) has been intensively studied by Electron Paramagnetic Resonance (EPR) spectroscopy also for its role of probe of the oxide surface in that the spectral features of this radical anion are sensitive to the ionic charge of the adsorption positive site.[18-20]

The superoxide radical ion in fact is a $13e^-$ π-radical containing three electrons in the $2\pi^*$ antibonding orbitals. The EPR features of this species (in the case of oxygen with natural isotopic composition) are limited to the g tensor which has been described, for O_2^- trapped in the bulk of KCl[21], using a totally ionic model. Adapting this model to an ionic superoxide symmetrically (side-on) interacting with a surface positive site (Scheme Ia), the g values in the three main directions of the reference system (neglecting second order approximation) are:

$$g_{xx} = g_e \; ; \quad g_{yy} = g_e + 2\lambda/E; \quad g_{zz} = g_e + 2\lambda/\Delta \quad (1)$$

where λ is the spin-orbit coupling constant for oxygen, Δ is the separation between the two π^* orbitals caused by the electric field of the adsorption site and E is the separation between the highest of the two π orbitals and the 2σ orbital. Taking into account that E is about one order of magnitude larger than Δ, the g_{zz} component (z is the direction of the internuclear oxygen axis) is the most sensitive one to the electric field exerted by the adsorption cationic site. In the approximation adopted the g_{xx} term (x is the direction perpendicular to the surface) coincides with the free spin value (g_e = 2.0023) and is practically independent from the nature and charge of the adsorption site.

In the case of cerium dioxide, the group of J. Soria and J.C. Conesa has used the EPR spectra of adsorbed superoxide to

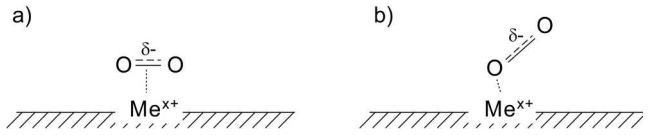

Scheme 1 Structure of the superoxide complexes; a) side-on mode; b) end-on mode.

explore the structure of the surface and to monitor the electron transfer properties of this solid after partial oxygen depletion.[22-24] A clear description of this partially reduced surface, in fact, is made difficult also by the impossibility to directly observe by EPR the paramagnetic Ce^{3+} ions due to the low relaxation time of this paramagnetic centre which causes a strong line broadening pushing the signal beyond the limit of detectability. The superoxide formation at the surface of partially reduced ceria occurs via electron transfer from Ce^{3+} ions:

$$O_{2(gas)} + Ce^{3+}_{(surf)} \rightarrow O_2^- - Ce^{4+}_{(surf)} \quad (2)$$

The O_2^- - Ce^{4+} surface complex on CeO_2 show peculiar properties as reported in several papers[22-24]. The g tensor structure of this species, in fact, is not amenable to the above described ionic model (eq. 1) because the g_{xx} component is found at values higher than g_e, i.e. around g=2.010 - 2.012. To explain this deviation from the ionic model (which applies, by the way, in the large majority of the surface superoxide species) the role of some coupling of the oxygen orbitals with the *f*-orbitals of the cerium ion (high spin-orbit coupling constant) has been invoked [25].

The process in equation 2 cannot be reversed in mild conditions (e.g. removing the oxygen atmosphere near room temperature) since reaction 2 is the first step of a process ending up in oxygen ions reincorporation in the solid. In other words further reduction of superoxide is favored in comparison with O_2 release.

The reversible fixation of oxygen at a substrate, nearly absent in gas-solid heterogeneous chemistry, has, however, enormous importance in biochemistry since the transport of oxygen in animal organisms is done by oxygen carriers, i.e. by proteins like Fe-hemoglobin capable to bind O_2 in an oxygen-rich atmosphere and to release the molecule when the atmosphere becomes oxygen-poor. This reversible oxygen fixation is also shown by some inorganic molecular systems based on transition metal ions (Co, Fe)[26, 27] and, to the best of our knowledge, was found, for solid systems, only in one case, the CoO-MgO solid solutions.[28-30] These solids can be defined heterogeneous oxygen carriers as, like their homogeneous and biochemical counterparts, they reversibly bind oxygen via a mechanism of electron donation and back-donation involving the orbitals of Co^{2+} and O_2 which is typical of coordination chemistry. Though in the above mentioned cases a non-negligible degree of electron transfer from the metal ion towards the oxygen molecule occurs, the metal-oxygen complex is totally different from the simple, ionically bonded, superoxide on top of a cation site. The latter is a symmetric moiety, side-on adsorbed on top of the cation, while molecular and heterogeneous oxygen carriers exhibit bent, end-on structure with a Me-O-O angle in the range 120°-140°. Scheme I compares the two described models. In the first case (Ia) the ionic interaction is usuallly non reversible. In the second one (Ib) the coordination bond typical of oxygen carriers corresponds to a reversible chemical interaction.

In the present paper we report an exciting example of superoxide ions generated by electron transfer (Eq. 2) found investigating the properties of CeO_2-TiO_2 mixed systems. We will show in the following that oxygen adsorbs on the activated (fully oxidized) material with formation of a ionic, symmetrically adsorbed superoxide anion. The reaction however is fully reversible at room temperature and the observed oxygen-Ce complex which has the typical structure of the complex in Scheme Ia, actually behaves like the typical reversible carriers schematized in Scheme Ib.

Materials and methods

Preparation of the samples

All reactants employed in this work were purchased by Aldrich and used without any further purification treatment.

Mixed Ti-Ce oxides were prepared via sol-gel synthesis following the procedure described by Fang *et al*[15]. For each sample a solution A was prepared stirring 10 g of $Ti(OC_4H_9)_4$, 3 ml of CH_3COOH and 40 ml of C_2H_5OH. The pH of this solution was adjusted to 2.3÷2.7 using HNO_3. Solution B was prepared with a stoichiometric amount of $Ce(NO_3)3 \cdot 6H_2O$, 3 ml of distilled water and 20 ml of C_2H_5OH. Solution B was added dropwise to solution A while stirring, until a stable sol was formed. This sol has been aged in air until the formation of a gel, then dried at 343K for 72 hours. Finally the powder was calcined at 723 K in air for 2 hours.

The concentrations of the mixed oxides prepared with the described procedure were 10% and 50% molar in CeO_2 : these materials will be hereafter labelled as CT10 and CT50 respectively.

Some properties of these mixed oxides were compared with those of a sol-gel prepared (starting from $Ce(OC_3H_7)_4$) CeO_2.

Prior to spectroscopic investigations (IR and EPR techniques) samples underwent an activation treatment consisting in a thermal annealing (1h at 573K under vacuum) aimed to remove surface impurities, followed by an oxidation step (2h at 773K in O_2 atmosphere) which allows the recovery of a fully oxidized state.

Characterization techniques

Powder X-rays diffraction (XRD) patterns were recorded with a PANalytical PW3040/60 X'Pert PRO MPD using a copper K_α radiation source (0.15418 nm). The intensities were obtained in the 2θ ranges between 20° and 70°. The X'Pert High-Score software was used for data handling.

The UV-Vis absorption spectra were recorded using a Varian Cary 5 spectrometer, coupled with an integration sphere for diffuse reflectance studies, using a Carywin-UV/scan software. A sample of PTFE with 100% reflectance was used as reference.

To perform FT-IR spectroscopy measurements the powdered samples were pressed into self supporting wafers and the spectra were acquired in transmission mode. The infrared spectra were recorded on a Bruker Equinox 55 FTIR spectrometer. 128 interferograms (recorded at 2 cm^{-1} resolution) were typically averaged for each spectrum.

Electron Paramagnetic Resonance (EPR) spectra, recorded at room temperature and at liquid nitrogen temperature, were run on a X-band CW-EPR Bruker EMX spectrometer equipped with a

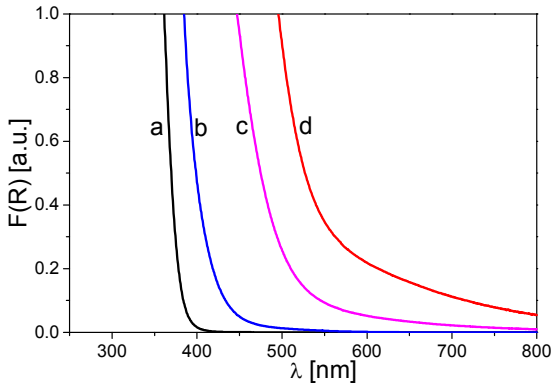

Fig. 1 Absorption spectra of TiO_2 (a), CeO_2 (b), CT10 (c) and CT50 (d)

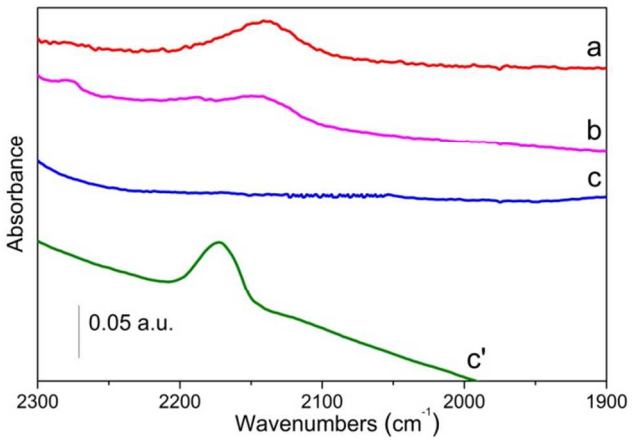

Fig. 2 FT-IR spectra, recorded at room temperature, of the activated samples. a) CT50, b) CT10, c)CeO_2. The trace c') correspond to CeO_2-red , a partially reduced ceria since the sample was annealed under vacuum at 773K and not reoxidized.

cylindrical cavity operating at 100 kHz field modulation and computer simulation of the spectra were obtained using the SIM32 programme developed by Prof. Sojka (Jagellonian University, Cracow, Poland[31]). EPR experiments at 4K were performed on an ELEXYS 580 Bruker spectrometer (at a microwave frequency of 9.76 GHz) equipped with a liquid-helium cryostat from Oxford Inc.

To perform the spin counting (number of paramagnetic species in a given sample) the integrated area of the EPR spectra were compared with those derived from a calibration curve obtained using a series of DPPH (2,2-Di(4-tert-octylphenyl)-1-picrylhydrazil) solutions in cyclohexane of known concentration.

RESULTS AND DISCUSSION

Characterization of CT materials

X-Ray Diffraction patterns

XRD patterns of the samples investigated in this work have been reported elsewhere[32]. Pure CeO_2 shows the typical peaks of the cubic fluoritic phase, with crystallites of about 12nm. CT10 is dominated by the peaks of TiO_2 (anatase phase) with crystallite size of about 14nm, with only a weak additional shoulder corresponding to the main peak of cubic ceria. Conversely the CT50 pattern is dominated by the peaks of the cubic CeO_2 phase with a shoulder corresponding to the main reflection of anatase. In this case the crystallites are very small being about 6nm for the cubic phase and even smaller for anatase.

Diffuse Reflectance UV-Vis Spectroscopy.

The Kubelka-Munk transformed spectra of both the mixed samples and the bare oxides are reported in Fig. 1. The mixed oxides have a significant red shift of their absorption edge with respect to the parent oxides due to the presence of Ce^{3+} at the interface between the two main phases. In fact a previous Raman work has identified the formation of some amount of a Ce(III) titanate ($Ce_2Ti_2O_7$) which has the pyrochlore structure and which is not enough abundant to be detected by X-ray diffraction in the two materials here considered. This phase is formed by solid state reaction at the interface between the two oxides. The strong red shift of the absorption edge shown by both CT10 and CT50 (fig. 1) with respect to both bare oxides is essentially due to the presence of this compound which has a pronounced brown colour.[33]

IR spectroscopy

Fig 2 compares the IR spectra of the two CT mixed materials with those of two CeO_2 samples one of which underwent the normal activation treatment described in Section 2 with final oxidation while the second was simply cooled upon the initial annealing at 773 K and therefore results partially reduced (CeO_2-red, Fig. 2c'). The IR trace of this partially reduced ceria (Fig.2c') shows a band at about 2170 cm^{-1}, which is absent in the re-oxidized sample (Fig. 2c). Signals in this spectral region have been already observed before[34] and ascribed to the forbidden $2F_{5/2} \rightarrow 2F_{7/2}$ electronic transition of Ce^{3+}.

The observed band can be therefore considered the finger print of Ce^{3+}whose presence is of course expected in reduced ceria. A similar band, though slightly broader and at slightly lower frequency is visible also in the spectra of CT10 and CT50 at the end of the oxidative activation in O_2 (Fig. 2 a and b). This confirms the presence of Ce^{3+} in mixed CT materials as already inferred on the basis of Raman results[35].

The reversible reduction of oxygen at the ceria-titania surface

EPR spectra of oxygen adsorbed on CeO_2-TiO_2 mixed materials

After the last phase (oxidation in O_2 at 773K) of the activation treatment and the final removal of the oxygen atmosphere at room temperature the EPR spectra of all materials (CT10, CT50, CeO_2) show a flat baseline. However, if a dose of oxygen (ca. 5-25 mbar) is admitted again onto the samples at room temperature, an EPR spectrum shows up in the case of the two mixed materials whereas no reaction occurs in the case of CeO_2. The EPR spectra recorded under oxygen have quite ill-defined profiles at RT but become clear and rather intense if recorded at 77K (Fig. 3). At this temperature the two spectra are similar to those already reported by Conesa and coworkers for differently prepared CT systems[36] and assigned to adsorbed superoxide ions. Surprisingly, the EPR spectrum vanishes if oxygen is removed by pumping off at RT and appears again if a new dose of oxygen is re-adsorbed. In other words oxygen is adsorbed in a totally reversible way by the two mixed materials producing a paramagnetic superoxide species whose spectral profile however is quite dissimilar from most frequently observed superoxides species and deserves

Cite this: DOI: 10.1039/c0xx00000x

www.rsc.org/xxxxxx

ARTICLE TYPE

Table 1 EPR parameters (g values and ^{17}O hyperfine structure tensors) of superoxide species

SAMPLE	g_{zz}	g_{yy}	g_{xx}	^{17}O A_{zz}	^{17}O A_{yy}/mT	^{17}O A_{xx}/mT	Ref.
CT10	2.0247	2.0205	2.0125	Unres.	7.5	Unres	This work
CT50	2.0256	2.0206	2.0126	Unres	7.6	Unres	This work
CeO_2	2.030	2.010		Unres	7.3		37

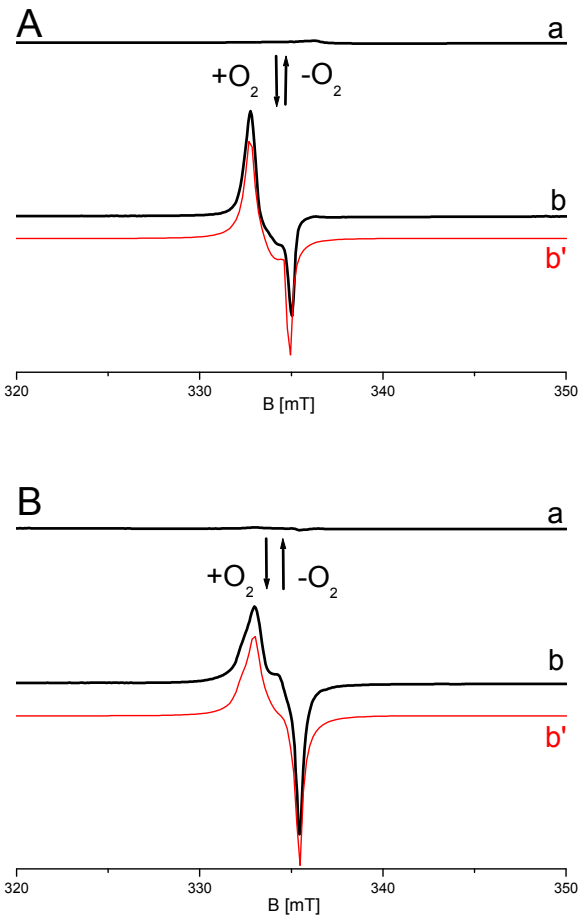

Fig. 3 EPR spectra (recorded at 77K) describing the effect of oxygen adsorption onto as prepared CT10 (A) and CT50 (B). a) baseline recorded under vacuum; b) after admission of 25 mbar O_2 at room temperature, experimental (b) and simulated (b') traces. The arrows between the two spectra outline the reversibility of the phenomenon.

further insights.

The computer simulations reported in Fig. 3 have been performed using the following values for the g tensor elements: g_{zz} = 2.0256 g_{yy}=2.0206 g_{xx}= 2.0126 (Table 1) and working in the rigid limit (i.e. without introducing dynamic effects to simulate the experimental profile). The g tensor parameters (see also fig. 5c) are compatible with an adsorbed superoxide species

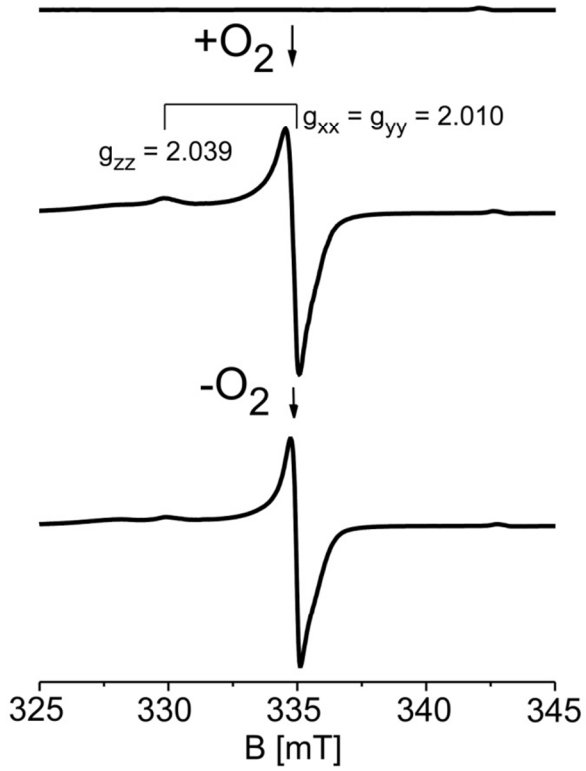

Fig. 4 EPR spectra (recorded at 77K) describing the effect of oxygen adsorption onto bare Cerium dioxide annealed at 673K for 4 hours.

and in particular the g_{xx} value, which is higher than 2.0023 and similar to that found in the case of ceria, indicates that Ce^{4+} is the adsorbing cationic site.

As already mentioned, bare CeO_2 behaves differently from CT materials. To observe superoxide formation on cerium dioxide it is necessary to adsorb O_2 onto an annealed, partially reduced, sample (CeO_2-red). This is shown, for sake of comparison, in Fig. 4 to evidence that: a) the EPR signal profile corresponding to the adsorbed superoxide on ceria[24] is different from that observed for mixed CT materials ; b) the adsorption, and the corresponding electron transfer, is not reversible by removing oxygen at RT.

The EPR signal in Fig. 4 has been already reported and widely discussed. It is enough, for our purposes, to notice that it has the typical quasi-axial lineshape of many adsorbed ionic superoxides with the g_{zz} component well evidenced at low field (g_{zz}= 2.039)

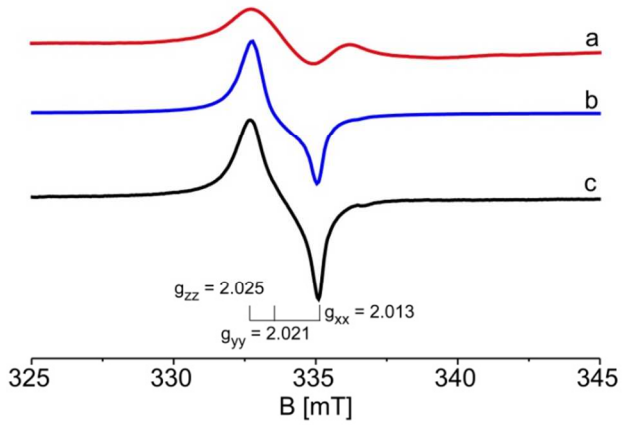

Fig. 5 EPR spectra of CT10 under oxygen (25mbar) at room temperature (a), 77K (b), 4.5K(c).

and the other two components merged in a unique unresolved line.

Compared to the superoxide spectra in fig. 4, those in fig.3 are quite unusual. The absence of dynamic effects causing partial averaging of the g tensor elements[38] is confirmed by analyzing the spectral shape at various temperatures. Fig. 5 shows the spectra of CT10 under oxygen (25mbar) recorded at room temperature, 77K and 4.5K respectively.

As it can be clearly seen from figure 5, by decreasing the recording temperature the linewidth also decreases but the lineshape is poorly affected and, considering the spectra at increasing T, there is no evidence of rotational effects causing averaging between different g tensor elements.

Spectra having shape similar to those here reported for CT materials were observed also in the case of CeO_2/Al_2O_3[14, 39, 40], CeO_2/SiO_2[25] and Cl-modified CeO_2[23]. However the original aspects of our investigation are the following: i) the spectra are formed by reaction of O2 with a fully oxidized material; ii) the oxygen interaction, with complete surface to oxygen electron transfer (see next section) is fully reversible at RT.

EPR spectra obtained by ^{17}O enriched O_2.

A further confirmation of the fact that we are monitoring a true ionic superoxide species comes from the spectra recorded using ^{17}O enriched oxygen in the experiment. Due to the nuclear spin (I=5/2) of the ^{17}O isotope, an hyperfine structure is given rise which provides further indications about the structure of the adsorbed moiety and about the spin density distribution.

The hyperfine structure (reported in figure 6 for CT50) is based on a main sextet (the only structure visible at low ^{17}O enrichment, Fig. 6A) centered in correspondence of the central component of the g-tensor (g_{yy} in table 1) amenable to both the (equivalent) ^{16}O-^{17}O and ^{17}O-^{16}O isotopomers and on a 11-line structure (which dominates the spectrum for high enrichment, Fig. 6B) due to the ^{17}O-^{17}O isotopomer. The correspondence between the central component of the g-tensor and the highest hyperfine coupling is unusual as, in most cases, the structure with highest A results centered on the lowest g component (g_{xx}). This peculiar feature has been already reported in the literature and, in some case, the central component was even relabeled as g_{xx}. To conclusively verify this point theoretical calculations on spin density distribution are essential.

The hyperfine splitting, in the y direction, is A_{yy} = 7.6 mT, the

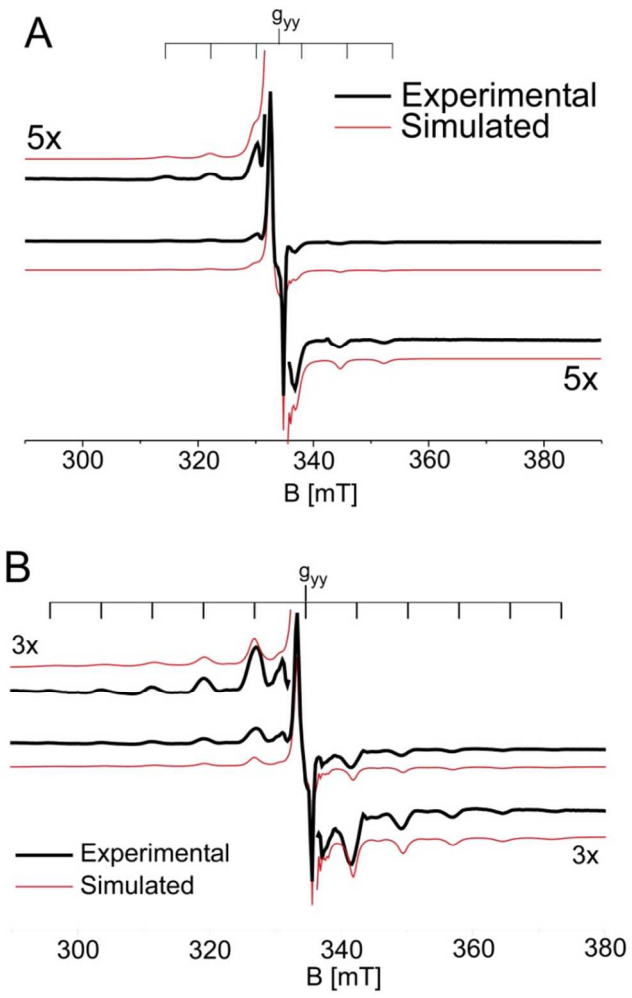

Fig. 6 EPR spectra (recorded at 77K) of superoxide species adsorbed on CT50 obtained using O_2 at different ^{17}O enrichments. Panel A: 28% isotopic enrichment; panel B: 90% isotopic enrichment.

two other components (A_{xx} and A_{zz}, which are expected to be much lower [41]) are unresolved. The structure of the $^{17}O_2$ spectra unambiguously indicates the presence of two magnetically equivalent oxygen atoms in the superoxide moiety[18, 41] exactly as observed in the case of pure CeO_2[25]. This points to the presence, also in our case, of a symmetric side-on moiety (Scheme Ia) and excludes the presence of an end-on superoxide adduct. The same result was found also in the case of CT10, with a A_{yy} hyperfine constant of 7.5mT. The hyperfine constant is the same observed for O_2^- on ceria[18] and its value allows to evaluate a spin density over the two oxygen atoms of about 98% (97% for CT10).

We are facing therefore an amazing results which can be resumed as follows. CeO_2-TiO_2 mixed materials (CT10, CT50) contain surface sites capable of adsorbing oxygen via electron transfer forming a true ionic superoxide ion, symmetrically adsorbed in side-on structure. Although the electron transfer from the solid is practically complete (97-98%), the reaction is fully reversible at room temperature and oxygen desorbs, by lowering the pressure, releasing the extra-electron to the solid. The g_{xx} parameter of the adsorbed superoxide has the same anomalous value found for CeO_2, fig. 4, indicating that the adsorption site is

a Ce^{4+} ion (eq. 2). Apart the nature of the adsorption centers, the behavior of the two systems is radically different.

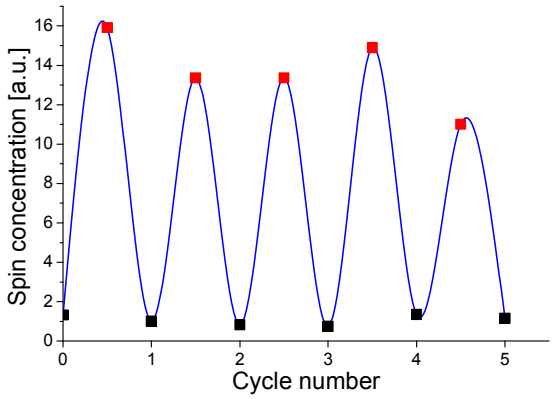

Fig. 7 Plot of the integrated area of the EPR signals for different cycles of adsorption/evacuation of 10mbar O_2 over CT50.

The electron transfer, in fact, is reversible in the case of CT materials and not reversible in the case of ceria and the spectra of adsorbed superoxide (compare Fig. 3 and 4) are surprisingly different one from each other.

The simple model of ionic adsorption (eq. 1) usually adopted by the surface chemistry of oxides must be discarded when analyzing the spectra of superoxide on CT samples because the requirements for such a model are not valid. In fact: i) g_{xx} deviates from g_e and ii) g_{zz} , in the case of CT is lower than in the case of ceria. This latter fact, according to the ionic approach, should indicate that O_2^- is more strongly bound in the case of CT samples which is evidently not the case.

The $O_2 + Ce^{3+} \rightleftarrows O_2^- - Ce^{4+}$ equilibrium in CT samples

As reported in the previous Sections, the superoxide formation on CT samples is reversible. To better illustrate this phenomenon, Figure 7 shows the result of a quantitative evaluation of adsorbed superoxide obtained using a spin counting approach, i.e. the double integration of the first-derivative EPR signals which is proportional to the number of paramagnetic species. This was done for successive cycles of adsorption-desorption (10 mbar of oxygen) on CT50. Despite some fluctuation due to unavoidable random factors, the behavior of the system indicates that the reversibility of the observed electron transfer goes well beyond the first cycle and that the observed interaction can be described in terms of the gas-solid equilibrium according to the following reaction:

$$O_{2(gas)} + Ce^{3+}_{(surf)} \rightleftarrows O^-_{2(ads)} - Ce^{4+}_{(surf)} \qquad (3)$$

We have also recorded EPR spectra under increasing oxygen pressure at constant temperature (RT) performing again, as in the case of Fig. 7, a quantitative analysis. In this case the area of each signal after double integration was compared with that of a DPPH standard in order to estimate the number of spins.

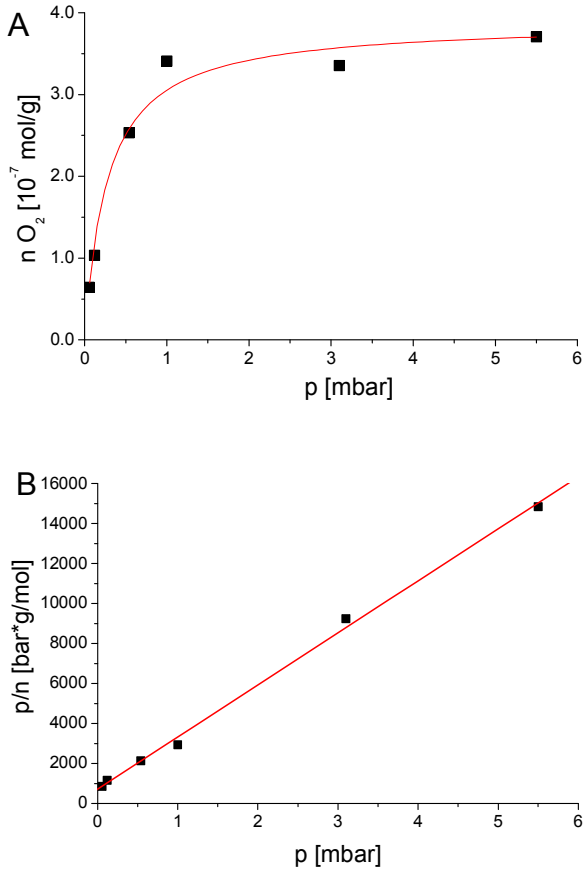

Fig. 8 Panel A: adsorption isotherm of O_2 on CT50.the adsorbed amount has been evaluated via double integration of the superoxide spectra. Panel B: Langmuir plot of the data in panel A.

The result of this experiment, a true "EPR adsorption isotherm", is reported in figure 8A where the number of adsorbed superoxide ions, n, is reported as a function of the O_2 equilibrium pressure.

The experimental points of Panel A reproduce a classic Langmuir adsorption isotherm since they nicely give a straight line when introduced into a Langmuir plot (8B) in which the p/n ratio is reported as a function of p following the equation:

$$\frac{p}{n} = \frac{1}{K_{eq} n_m} + \frac{p}{n_m} \qquad (4)$$

where n_m is the number of moles adsorbed at full coverage, K_{eq} is the equilibrium constant, p is the pressure and n is the number of adsorbed moles. From this linearization it is possible to evaluate the maximum amount of adsorbed oxygen over 1g of sample: $n_m=3.8\cdot10^{-7}$ mol; and the adsorption equilibrium constant: $K_{eq}=3606$. Using then:

$$\Delta G^0 = -RT\ln K_{eq} \qquad (5)$$

the Gibbs free energy of formation can be computed. The value found for this system is $\Delta G^0=-20$KJ/mol, which is consistent with both the spontaneous formation of these species and the reversibility of the adsorption.

Conclusions

Two mixed CeO_2-TiO_2 solids with different composition show a peculiar surface reactivity because they react, in their fully oxidized state, with oxygen producing an adsorbed superoxide by direct electron transfer. The reaction is pressure dependent and completely reversible showing the behavior typical of natural and synthetic oxygen carriers even if the structural features of the adsorbed oxygen (side-on, symmetrically adsorbed on a Ce site) are totally different from those shown by oxygen carriers (end-on bent adducts coordinate to a transition metal ion) and closely resemble to those of a plethora of superoxide adsorbed on the surface of metal oxides.

The sites of cerium capable of the electron transfer do not belong to the CeO_2 phase because the pure oxide does not show the described behavior and does not contain, unless annealed with oxygen depletion, Ce^{3+} ions. The active sites must therefore be sought in that part of the system where the oxide-oxide interaction led to the creation of new or modified phases. The CeO_2-TiO_2 mixed oxides appear, at a first sight, as an heterogeneous mixture of crystals of the two oxides which are, however, very intimately combined. The absence of a mutual solubility in the highest oxidation state (Ce^{4+}, Ti^{4+}) is substituted by a reactivity at the interface which leads to the partial formation of a novel stoichiometric compound, $Ce_2Ti_2O_7$, having pyrochlore structure. In this compound cerium and titanium ions coexist but cerium is present as Ce^{3+} ion in the fully stoichiometric phase. Previously published XPS data confirm the presence of Ce^{3+} in both mixed oxides (CT10, CT50) showing that a fraction of these ions is at the surface or near the surface[32]. The FT-IR spectra reported here are a further confirmation of this idea, since they show the presence of Ce^{3+} ions on the fully oxidized samples.

Ce^{3+} ions are octacoordinated in the pyrochlore structure. Those responsible for the investigated interaction must be firstly searched at the surfaces of this mixed phase where sites with lower coordination likely may have the geometric and electronic arrangement for binding oxygen in the described way. Theoretical modeling of the possible situations originated in this complex and heterogeneous systems are needed to advance toward a full identification of the nature of the active site. Despite this partial uncertainty on the exact location of the Ce^{3+} active site, the observation reported here opens innovative perspectives both in the field of heterogeneous catalysis (the reductive activation of oxygen occurs on a fully oxidized undefective solid) and in the field of sensors as the total reversibility of the electron transfer is observed in a significant range of oxygen pressure.

Acknoledgements

This work has been supported by the Italian Ministry of University and Research, MIUR, through the "Programs of National Relevance" (PRIN 2010-2011:prot. 2010FPTBSH_003); the "National Funding for Basic Research" (FIRB) with a project entitled "Oxides at the nanoscale: functionalities and applications" (FIRB RBAP11AYN), and by a Marie Curie International Research Staff Exchange Scheme Fellowship (PHOTOMAT, proposal n. 318899) within the 7th European Community Framework Programme. We are also indebted to the COST action CM1104 "Reducible oxides".

Notes and references

[a] *Dipartimento di Chimica and NIS, Università degli Studi di Torino, Via Pietro Giuria 7 , 10125, Torino, Italy. Tel: +39 011 6707576; E-mail: mariacristina.paganini@unito.it*

1 A. Bielanski and J. Haber, *Oxygen in Catalysis*, Marcel Dekker, Inc., New York, 1991.

2 J. Kaspar, P. Fornasiero and M. Graziani, *Catal. Today*, 1999, **50**, 285-298.

3 S. Abdollahzadeh-Ghom, C. Zamani, S. Nazarpour, T. Andreu and J. R. Morante, *Sens. Actuators, B*, 2009, **140**, 216-221.

4 G. Balducci, P. Fornasiero, R. Dimonte, J. Kaspar, S. Meriani and M. Graziani, *Catal. Lett.*, 1995, **33**, 193-200.

5 N. Izu, T. Omata and S. Otsuka-Yao-Matsuo, *J. Alloys Compd.*, 1998, **270**, 107-114.

6 C. K. Krishnan, K. Nakamura, H. Hirata and M. Ogura, *Phys. Chem. Chem. Phys.*, 2010, **12**, 7513-7520.

7 A. Martinez-Arias, M. Fernandez-Garcia, C. Belver, J. C. Conesa and J. Soria, *Catal. Lett.*, 2000, **65**, 197-204.

8 B. M. Reddy and A. Khan, *Catal. Surv. Asia*, 2005, **9**, 155-171.

9 T. Montini, M. A. Banares, N. Hickey, R. Di Monte, P. Fornasiero, J. Kaspar and M. Graziani, *Phys. Chem. Chem. Phys.*, 2004, **6**, 1-3.

10 T. Montini, N. Hickey, P. Fornasiero, M. Graziani, M. A. Banares, M. V. Martinez-Huerta, I. Alessandri and L. E. Depero, *Chem. Mater.*, 2005, **17**, 1157-1166.

11 P. R. Shah, T. Kim, G. Zhou, P. Fornasiero and R. J. Gorte, *Chem. Mater.*, 2006, **18**, 5363-5369.

12 P. Vidmar, P. Fornasiero, J. Kaspar, G. Gubitosa and M. Graziani, *J. Catal.*, 1997, **171**, 160-168.

13 J. R. Gonzalez-Velasco, M. A. Gutierrez-Ortiz, J. A. Botas, S. Bernal, J. M. Gatica and J. A. Perez-Omil, in *Catalyst Deactivation 1999*, ed. B. Delmon and G. F. Froment, 1999, vol. 126, pp. 187-194.

14 M. Haneda, T. Mizushima and N. Kakuta, *J. Chem. Soc., Faraday Trans.*, 1995, **91**, 4459-4465.

15 J. Fang, X. Bi, D. Si, Z. Jiang and W. Huang, *Appl. Surf. Sci.*, 2007, **253**, 8952-8961.

16 S. Watanabe, X. Ma and C. Song, *J. Phys. Chem. C*, 2009, **113**, 14249-14257.

17 H. Yang, K. Zhang, R. Shi and A. Tang, *J. Am. Ceram. Soc.*, 2007, **90**, 1370-1374.

18 M. Che and A. J. Tench, *Adv. Catal.*, 1983, **32**, 1-148.

19 M. Che, E. Giamello and A. J. Tench, *Colloids Surf.*, 1985, **13**, 231-248.

20 M. Anpo, M. Che, B. Fubini, E. Garrone, E. Giamello and M. C. Paganini, *Top. Catal.*, 1999, **8**, 189-198.

21 W. Kanzig and M. H. Cohen, *Phys. Rev. Lett.*, 1959, **3**, 509-510.

22 A. Martinez-Arias, J. Soria, J. C. Conesa, X. L. Seoane, A. Arcoya and R. Cataluna, *J. Chem. Soc., Faraday Trans.*, 1995, **91**, 1679-1687.

23 J. Soria, J. C. Conesa and A. Martinez-Arias, *Colloids Surf., A*, 1999, **158**, 67-74.

24 J. Soria, A. Martinez-Arias and J. C. Conesa, *J. Chem. Soc., Faraday Trans.*, 1995, **91**, 1669-1678.

25 M. Che, J. F. J. Kibblewhite, A. J. Tench, M. Dufaux and C. Naccache, *J. Chem. Soc., Faraday Trans. I*, 1973, **69**, 857-863.

26 R. D. Jones, D. A. Summerville and F. Basolo, *Chem. Rev.*, 1979, **79**, 139-179.

27 T. D. Smith and J. R. Pilbrow, *Coord. Chem. Rev.*, 1974, **13**, 173-278.

28 E. Giamello, Z. Sojka, M. Che and A. Zecchina, *J. Phys. Chem.*, 1986, **90**, 6084-6091.

29 M. Che, K. Dyrek, E. Giamello and Z. Sojka, *Z. Phys. Chem. Neue Fol.*, 1987, **152**, 139-148.

30 Z. Sojka, E. Giamello, M. Che, A. Zecchina and K. Dyrek, *J. Phys. Chem.*, 1988, **92**, 1541-1547.

31 A. Adamski, T. Spalek and Z. Sojka, *Res. Chem. Intermed.*, 2003, **29**, 793-804.

32 C. Gionco, M. C. Paganini, S. Agnoli, A. E. Reeder and E. Giamello, *J. Mater. Chem. A*, 2013, **1**, 10918-10926.

33 M. Martos, B. Julian-Lopez, J. Vicente Folgado, E. Cordoncillo and P. Escribano, *Eur. J. Inorg. Chem.*, 2008, 3163-3171.

34 C. Binet, A. Badri and J. C. Lavalley, *J. Phys. Chem.*, 1994, **98**, 6392-6398.

35 C. Gionco, M. C. Paganini, E. Giamello, R. Burgess, C. Di Valentin and G. Pacchioni, *Chem. Mater.*, 2013, **25**, 2243-2253.

36 J. M. Coronado, A. J. Maira, A. Martinez-Arias, J. C. Conesa and J. Soria, *J. Photochem. Photobiol., A*, 2002, **150**, 213-221.

37 L. Mendelovich, H. Tzehoval and M. Steinberg, *Appl. Surf. Sci. (1977-1985)*, 1983, **17**, 175-188.

38 M. Shiotani, G. Moro and J. H. Freed, *J. Chem. Phys.*, 1981, **74**, 2616-2640.

39 A. Martinez-Arias, M. Fernandez-Garcia, L. N. Salamanca, R. X. Valenzuela, J. C. Conesa and J. Soria, *J. Phys. Chem. B*, 2000, **104**, 4038-4046.

40 A. Aboukais, E. A. Zhilinskaya, J. F. Lamonier and I. N. Filimonov, *Colloids Surf., A*, 2005, **260**, 199-207.

41 M. Chiesa, E. Giamello, M. C. Paganini, Z. Sojka and D. M. Murphy, *J. Chem. Phys.*, 2002, **116**, 4266-4274.